Composites: Part A 162 (2022) 107146

Contents lists available at ScienceDirect

Composites Part A

journal homepage: www.elsevier.com/locate/compositesa

4D printing of shape-changing structures based on IPN epoxy composites formed by UV post-curing and γ-ray radiation

Linlin Wang, Fenghua Zhang, Shanyi Du, Jinsong Leng *

Centre for Composite Materials and Structures, Harbin Institute of Technology (HIT), No. 2 Yikuang Street, Harbin 150080, People's Republic of China

ARTICLE INFO

Keywords:
A. Polymer-matrix composites
A. Smart materials
B. Mechanical properties
E. 3-D Printing

ABSTRACT

The cross-linking degree is a significant factor affecting the thermodynamic properties of resins, the cross-linking degree of photosensitive resins is limited during Digital Light Procession (DLP) printing. We present a strategy for double networks in epoxy resin to further improve the performances of printed structures via two different processing methods. Epoxy acrylates and polyethylene glycol dimethacrylates crosslink by UV-light radiation forming a light-induced network structure, and epoxy molecules crosslink under γ-ray radiation forming a ray-induced network structure. The two kinds of networks interpenetrate to form the interpenetrating polymer network (IPN). The printed IPN specimens have the characteristics of high Young's modulus (up to 4.89 GPa) and fracture strain (as high as 30.4 %). The printed flowers and canister reinforced by short glass fibers (GFs) exhibited rapid shape recovery behaviors. The IPN epoxy/GFs composites have good values in manufacturing smart deployable structures, medical devices, and automobile shell parts.

1. Introduction

Shape memory polymers (SMPs) are a new kind of intelligent material, which can restore temporary shapes to their original shapes under the stimulation of external conditions. The common thermosetting shape memory polymers are epoxy, cyanate ester, polyimide, bismaleimide, phenol–formaldehyde resin, and acrylate. The characteristics of shape memory epoxy are low cost, ease of processing, corrosion resistance, electric insulation, and excellent thermal and mechanical properties. It is widely used in aerospace, electronics, auto industry, architecture, sports equipment, coating, and adhesive fields. The significant drawbacks of the un-modified epoxy resin, including poor toughness and low strength, restrict its engineering applications.

There are many published works on the reinforcing and toughening of epoxy. The toughening mechanisms of epoxy resins are summarized into three categories. The first method is to reduce crosslinking density, the second is the chemical modification of main chains to decrease segment mobility, and the third is to add a ductile phase, such as carboxyl-terminated butadiene-acrylonitrile and amine-terminated butadiene-acrylonitrile [1–6]. All these approaches can achieve the purpose of toughness, but they also reduce the strength and thermal stability of the resins. Therefore, an appropriate strategy for epoxy resin with high strength and toughness is highly anticipated. A new solution to the above problem is constructing IPN in the resin. IPN consists of two or more polymer networks that are individually cross-linked and mutually penetrating, which can reinforce and toughen polymers [7–10]. We mapped out the strategy for forming IPN in epoxy resin. The first network is formed by UV-light radiation and then the second network is formed by γ-ray radiation. The toughening can be achieved without sacrificing the strength and thermal properties of the resin via the formation of the IPN in the resin.

In addition, complex structures of IPN toughened epoxy can be molded by combining the above strategies with DLP printing technology. DLP printing has the advantages of high printing speed and precision, which can print small and complex structures. DLP printer works in a layer-by-layer curing mode. The time to print a layer needs a few seconds or tens of seconds [11–15]. We set the layer time of 1 s to print structures resulting in incomplete cross-linking reactions of the acrylates and a low degree of cross-linking. The printed structures are reinforced by UV post-curing to improve the structures' cross-linking degrees and thermodynamic properties [16–20]. Epoxy requires higher energy to improve the crosslinking further. γ-rays transfer power to the irradiated material by ionization producing radicals and the radicals initiate cross-linking reactions [21,22]. At present, the influences of UV and γ-ray radiations on the properties of materials are rarely studied, especially systematic studies on the thermodynamic properties and shape memory

* Corresponding author.
E-mail address: lengjs@hit.edu.cn (J. Leng).

https://doi.org/10.1016/j.compositesa.2022.107146
Received 6 May 2022; Received in revised form 5 August 2022; Accepted 12 August 2022
Available online 17 August 2022

properties under different UV radiation times and different γ-ray doses.

We studied the preparation and printing process of epoxy-based inks and CNTs-doped and CFs-doped composite inks. We found that post-curing is a feasible method to enhance the thermodynamic properties of the resins and the efficiency of DLP printing in our previous work [23]. The reaction of epoxy and acrylic acid produces epoxy acrylate, the reaction's yield is about 68 %. Polyethylene glycol dimethacrylate (PEGDMA) is used as a thinner to regulate the viscosity of the ink, so the printing ink is a mixture of epoxy acrylate, PEGDMA, and epoxy. Epoxy acrylate and PEGDMA crosslink by UV lights to form the light-induced network, and epoxy molecules crosslink by γ-rays to form the ray-induced network. The two networks interpenetrate to strengthen and toughen the resin.

2. Experiments and characterizations

2.1. Materials and the preparation of printable inks

Bisphenol A epoxy resin was purchased from Nantong Xingchen Synthetic Materials Co. Ltd., China. PEGDMA, Acrylic acid, Triethylamine (TEA), Toluhydroguinone (THQ), and 2,4,6-Trimethylbenzoyldiphenyl Phosphine Oxide (TPO) were provided by Aladdin. All reagents were used as received.

0.4 mol acrylic acid and 0.2 mol epoxy resin reacted and stirred at a constant speed at 75 °C, and the reaction was catalyzed by TEA and THQ for 6 h. 0.07 mol PEGFDMA was added to dilute the synthetic and 2.0 wt % photoinitiator, TPO, was dissolved into the mixture to obtain the epoxy-based printable ink. 0.2 wt%, 0.5 wt%, and 1.0 wt% GFs were added to the ink to obtain composite inks.

2.2. DLP printing and UV post-curing

The photosensitive epoxy-based ink was shaped by a DLP printer. The printed specimens were washed and post-cured by a wash & cure machine (Anycubic, China). The rated power of the machine light source is 40 W and the wavelength of that is 405 nm. The specimens under different post-curing times (0 min, 2 min, 5 min, 10 min, 20 min, 40 min, 60 min, 90 min) were labeled PP0, PP2, PP5, PP10, PP20, PP40, PP60, and PP90, respectively.

2.3. γ-ray radiation

The post-cured specimens were radiated by different doses of γ-rays (0 KGy, 10 KGy, 100 KGy, 1000 KGy) produced by a ^{60}Co radiation source and labeled PPx-IRy (x = 0, 2, 5……; y = 0, 1, 2, 3). The experiments were carried out at the Heilongjiang Academy of Sciences (Harbin, China).

2.4. Cross-linking degree

The size of printed specimens used to test cross-linking degrees is 80 mm * 10 mm * 1 mm. The specimens with different exposure times were weighted and recorded as m_1, and soaked in acetone for 72 h. Then they were dried at 80 °C for 2 h. The oven-dried specimens were weighed again and recorded as m_2. The cross-linking degree (D_c) is calculated by the equation below:

$$D_c = \frac{m_1}{m_2} \times 100\% \tag{1}$$

2.5. Characterizations

The glass transition temperatures of the samples were tested using the differential scanning calorimeter (DSC, METTLER-TOLEDO Corporation, Switzerland) with a 10 °C/min ramp rate and a dynamic mechanical analyzer (Q800TA Corp., US) with a 3 °C/min ramp rate and a 1 Hz frequency. Thermogravimetry analysis (TGA) was carried out using an analyzer (Mettler-Toledo, Switzerland) from 25 °C to 800 °C with a 10 °C/min ramp rate in high purity N_2 atmosphere. Zwick/Roell Z010 (Zwick GmbH & Co. KG) Instrument was used to conduct the tensile test at room temperature with a 2.0 mm/min strain rate. At least three samples were tested for one formula. The surface and cross-section morphologies of the samples were exposed using a scanning electron microscope (SEM) (JSM-7600F, JEOL Ltd.). The samples were sputtered with gold for 30 s before observation. Fourier Transform Infrared Spectroscopy (FTIR) tested by the infrared spectrometer (Perkin Elmer Corp., US) was used to analyze the changes in functional groups in the samples.

2.6. Shape memory performances

The cycling shape memory behavior of the samples was characterized by a tensile fixture of the dynamic mechanical analyzer in controlled-force mode. The instrument recorded the samples' real-time force, displacement, and temperature. The following equations were used to calculate the shape fixity rate (R_f) and shape recovery rate (R_r) of every cycle.

$$R_f = \frac{\varepsilon - \varepsilon_0}{\varepsilon_{max} - \varepsilon_0} \times 100\% \tag{2}$$

$$R_r = \frac{(\varepsilon - \varepsilon_0) - (\varepsilon_{rec} - \varepsilon_0)}{(\varepsilon - \varepsilon_0)} \times 100\% \tag{3}$$

where ε_0 is the initial strain produced by a change in temperature, ε_{max} is the maximum strain under load, ε is the fixed strain after cooling and load removal, and ε_{rec} is the strain after recovery.

3. Results

The printable ink is a mixture of epoxy acrylate, epoxy, and PEGDMA. To improve DLP printing efficiency, the layer exposure time is set up for 1 s. The short exposure time can shape the ink, but the ink cannot be fully cross-linked in such a short time. UV post-curing treatment of the printed specimens is necessary. The specimens printed by the DLP printer were exposed to 405 nm UV lights of the wash & cure machine at different times. Their cross-linking degrees are calculated by the mass ratio before and after soaking, which are exhibited in Fig. 1(a-b). The cross-linking degree jumps from 86.6 % to 90.7 % in two minutes and rises slowly, indicating that the unreacted allyl groups in the polymer are quickly cross-linked. When the post-curing time is 60 min, it reaches 93.7 % and cannot be improved significantly with the increasing exposure time. Therefore, a post-curing time of 60 min is sufficient for the printed specimens.

Four specimens with UV post-curing treatment of 0 min, 5 min, 20 min, and 60 min were exposed to different doses of γ-rays. There was no significant change in the color of the specimens irradiated by 10KGy and 100 KGy γ-rays. At the same time, the specimens irradiated by 1000 KGy γ-rays change from light yellow to light brown. The discoloration may be due to over-curing caused by the high dose γ-rays.

The mechanism of polymerization and over-curing of the epoxy acrylate is demonstrated in Fig. 2. The photoinitiator, TPO, is irradiated by UV lights to produce free radicals, which initiate a chain reaction leading to the polymerization of the epoxy acrylate. An epoxy acrylate molecule contains two allyl groups, one allyl group is polymerized and the other allyl group is polymerized in the same way forming the resin with a 3D network structure finally. When the resin is radiated by 1000 KGy γ-rays, polyacrylate is destroyed and degraded to produce radical sub-products. Some C-O and C = O in the resin are easily broken to produce free radicals by γ-ray radiation, which are shown in red boxes. These radicals are free to recombine within themselves, oxygen or hydrogen resulting in the yellowing of the resin [24,25].

The formation and appearance of IPN are shown in Fig. 3. The UV

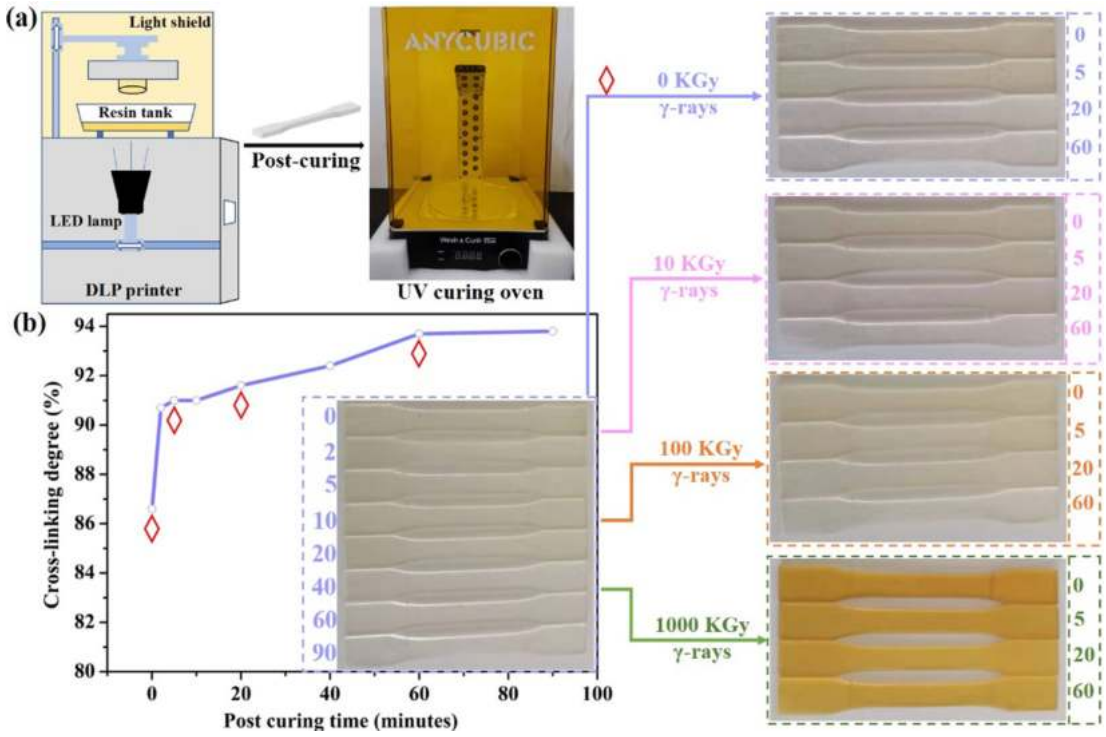

Fig. 1. (a) DLP printer and UV curing oven, (b) The cross-linking degrees of specimens under different UV post-curing times and the post-cured specimens irradiated by different doses of γ-rays. (For interpretation of the references to colour in this figure legend, the reader is referred to the web version of this article.)

light-induced network was initially formed during DLP printing and fully developed in the process of UV post-curing. The UV light-induced network was formed by polymerizing epoxy acrylate and PEGDMA and labeled "Network #1" in the figure. Then, the post-cured specimens are irradiated by γ-rays. The epoxy reacted forming the ray-induced network in the resin which was labeled "Network #2". The two networks interpenetrate with each other forming the IPN [26–28].

3.1. The effects of UV post-curing and γ-ray radiation on the thermal properties of the specimens

DSC results of the post-cured and irradiated specimens are shown in Fig. 4. There is a distinct step in the DSC curve. The temperature at which the tangent from the midpoint of the oblique line intersects the front baseline is the onset T_g [29–31], which is marked above the corresponding step.

The T_g of PP0-IR0 increases from 56.6 °C to 73.7 °C with the increasing UV post-curing time and the T_g of PP0-IR1 and PP0-IR2 show a similar increasing trend. Compared to PPx-IR0 (x = 0, 5, 20, 60), the T_g of PPx-IR1 (x = 0, 5, 20, 60) have no significant change, and that of PP20-IR2 and PP60-IR2 show a marked increase. The increase indicates that 100 KGy γ-rays contribute to the cross-linking reaction of epoxy in the resin. Among PP60-IRy (y = 0, 1, 2, 3), the T_g of PP60-IR2 is 82.6 °C and is the highest, demonstrating that a new network is formed after 100 KGy γ-ray radiation. However, the T_g of PP60-IR3 decreases compared with PP60-IR2, which a combination of polymerization and degradation might cause [32,33].

The weight-temperature curves of all specimens are shown in Figure S1. The weight loss is slow in the first stage of the TGA curves, which is caused by the release of small molecules in the resin. The initial decomposition temperature, labeled $T_{5\%}$, may indirectly reflect the cross-linking degree of molecular chains in the resin, which is exhibited in Table S1. For PPx-IR0 (x = 0, 5, 20, 60), the longer the UV post-curing time is, the higher the $T_{5\%}$ is. The $T_{5\%}$ of PP60-IR0 is up to 354.7 °C, 54.1 °C higher than that of PP0-IR0, which is caused by UV post-curing. The $T_{5\%}$ of PP60-IR0 decreases with the increase of γ-ray dose illustrating that γ-ray radiation accelerates the loss of small molecules. The $T_{5\%}$ of PPx-IR1 (x = 0, 5, 20, 60) is the highest and that of PPx-IR3 (x = 0, 5, 20, 60) is the lowest among all the irradiated resins, which demonstrates that 1000 KGy γ-rays harm the thermostability of the resins, resulting in degradation. The thermal degradation rates depend on the resins' crosslinking degree, which seems in agreement with the DSC result.

3.2. The effects of UV post-curing and γ-ray radiation on the mechanical properties of the specimens

DMA can also test T_g of the specimens, and the curves of tan δ and storage modulus are shown in Figure S2. The data are listed in Table S2 and S3. The 3D bar graphs are shown in Fig. 5 and the changes in T_g and storage modulus (at 30 °C) can be observed in the charts. The T_g of PPx-IR0 (x = 0, 5, 20, 60) increases from 50.3 °C to 65.7 °C with the increasing UV post-curing time, which is similar to the DSC result. The increase is caused by the formation of the UV light-induced network that increases the cross-linking degree of the resin. The T_g of PP0-IRy (y = 0, 1, 2, 3) shows significant growth from 50.3 °C to 71.5 °C, which is caused by the formation of the IPN network triggered by γ-ray radiation. The T_g of PP60-IRy (y = 0, 1, 2, 3) shows a slight increase of 2.9 °C after 1000 KGy γ-ray radiation. The 1000 KGy γ-rays have two different effects on resin: to promote the formation of the cross-linking network structure and to destroy the network structure. The combination of these two effects causes the slight increase.

The storage modulus of PP0-IRy (y = 0, 1, 2, 3) increases from 525.4 MPa to 2530.7 MPa with the increasing γ-ray dose. The storage modulus of PPx-IR0 (x = 0, 5, 20, 60) increases from 525.4 MPa to 3124.3 MPa with the increasing UV post-curing time. The increase demonstrates that both UV post-curing and γ-ray irradiation are beneficial to further cross-linking of the resin. Among PP60-IRy (y = 0, 1, 2, 3), the storage modulus of PP60-IR2 is the highest, up to 4894.3 MPa, which is attributed to the formation of the ray-induced network. The storage

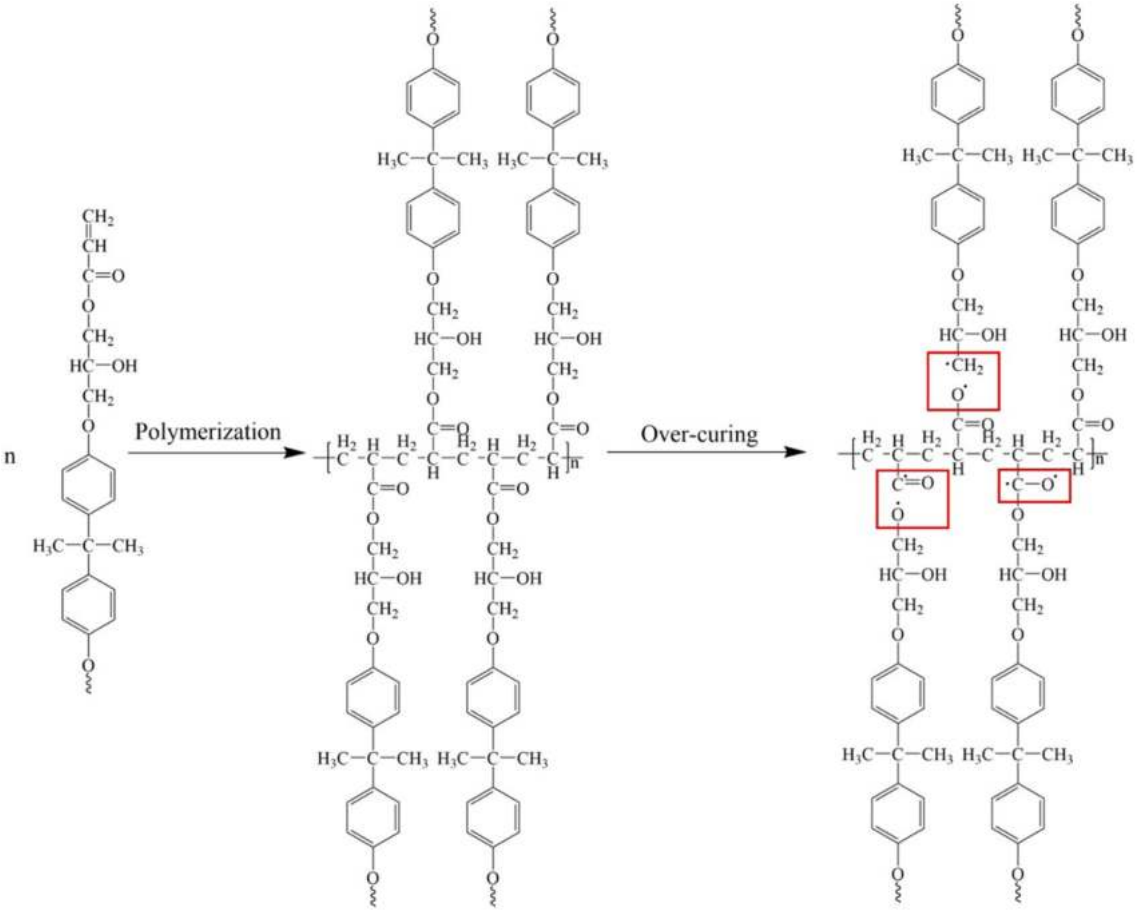

Fig. 2. Polymerization and over-curing of the epoxy acrylate. (For interpretation of the references to colour in this figure legend, the reader is referred to the web version of this article.)

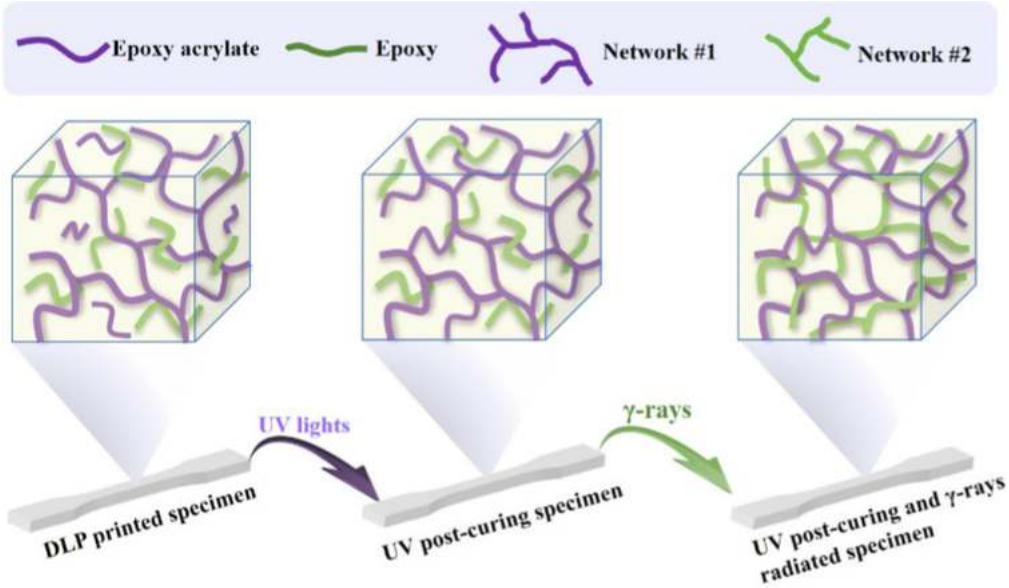

Fig. 3. The formation of IPN in the post-cured and irradiated specimens. (For interpretation of the references to colour in this figure legend, the reader is referred to the web version of this article.)

modulus of PP60-IR3 is 2587.3 MPa, and the decline is mainly caused by the resin degradation by 1000 KGy γ-ray radiation. The variation of PP60-IRy (y = 0, 1, 2, 3) in storage modulus is consistent with that in T_g.

Stress–strain behavior is an important indicator in evaluating the mechanical properties of the specimens. The stress–strain curves of all specimens irradiated by UV light and γ-rays are shown in Fig. 6 and the

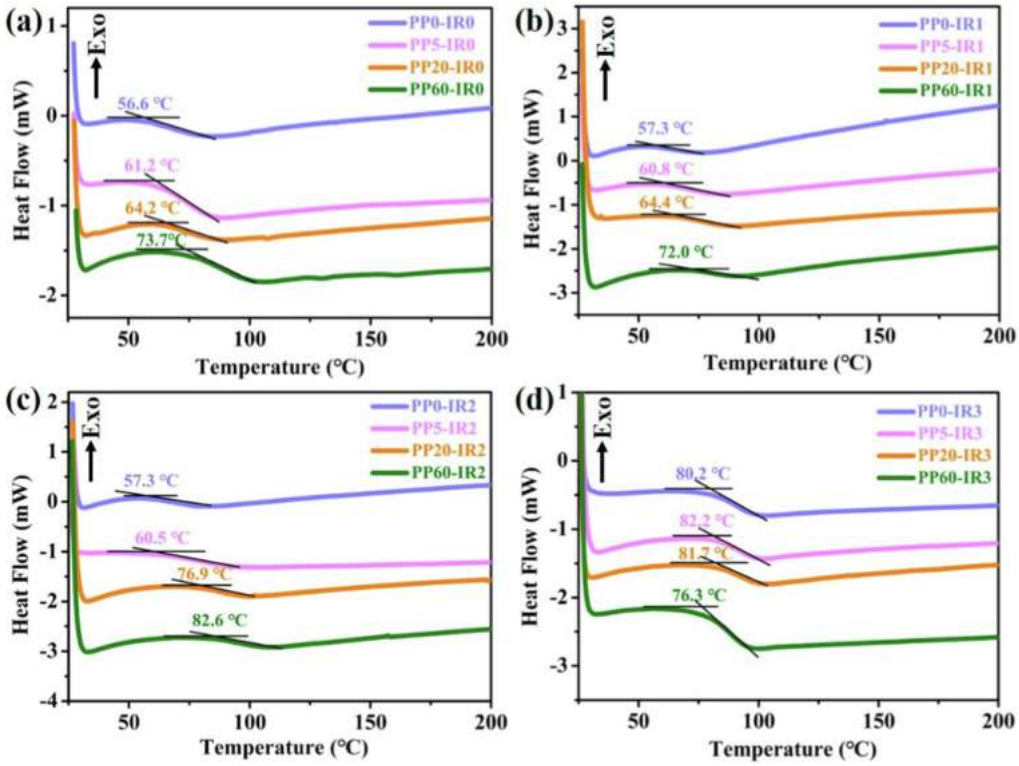

Fig. 4. T_g of the post-cured and irradiated specimens tested by DSC. (For interpretation of the references to colour in this figure legend, the reader is referred to the web version of this article.)

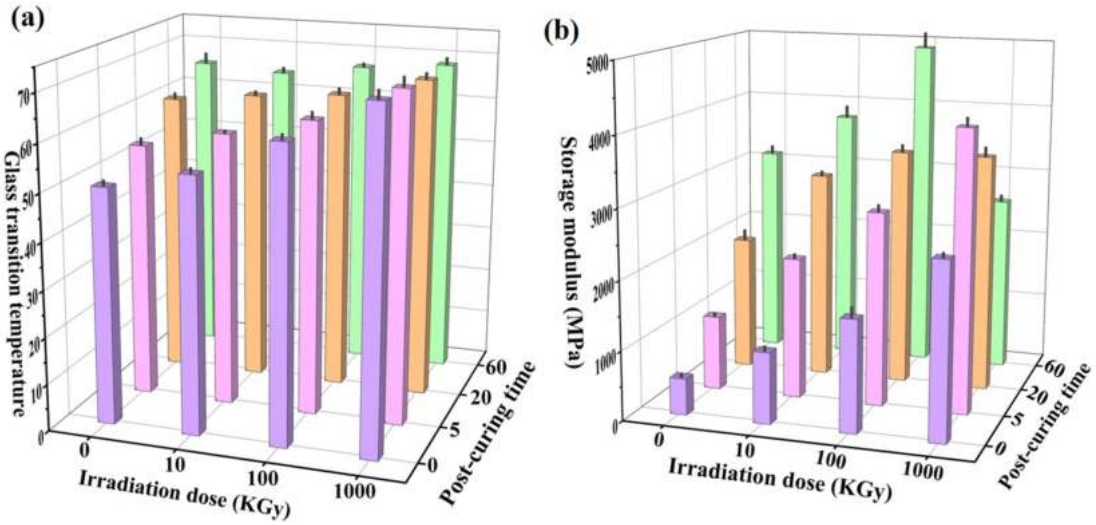

Fig. 5. T_g and storage modulus of the post-cured and irradiated specimens. (For interpretation of the references to colour in this figure legend, the reader is referred to the web version of this article.)

data on fracture strain and stress are listed in Table S4 and S5. The fracture strain of PPx-IR0 (x = 0, 5, 20, 60) decreased gradually from 28.5 % to 18.4 % with the increase of UV post-curing time. It is noteworthy that the shape of the stress–strain curve changed significantly. For PP0-IR0, the relationship between stress and strain is almost linear, and elastic deformation occurs. For PP60-IR0, the tensile stress increases to a maximum value, then decreases. The specimen is further stretched, its deformation concentrated in the material's necking area, and finally, the specimen is broken. The increase in fracture stress and decrease in fracture strain is mainly due to the high cross-linking degree of the specimen. The changes of PPx-IR1 (x = 0, 5, 20, 60) and PPx-IR2 (x = 0, 5, 20, 60) are similar to those of PPx-IR0 (x = 0, 5, 20, 60). The fracture stress increases and the fracture strain decreases. The stress–strain relationship of PPx-IR3 (x = 0, 5, 20, 60) was almost linear indicating that brittle fracture occurred in the specimens. The photos of PP60-IR2 and PP60-IR3 being pulled apart are displayed in Figure S3. Among all specimens, the fracture strain of PPx-IR3 (x = 0, 5, 20, 60) is the lowest. It is significantly lower than that of other samples demonstrating that 1000 KGy γ-rays damage the specimens' network structures leading to stress concentration and fracture during stretching. From the results of the DMA and tensile tests, the mechanical property of PP60-IR2 is the most outstanding among all specimens.

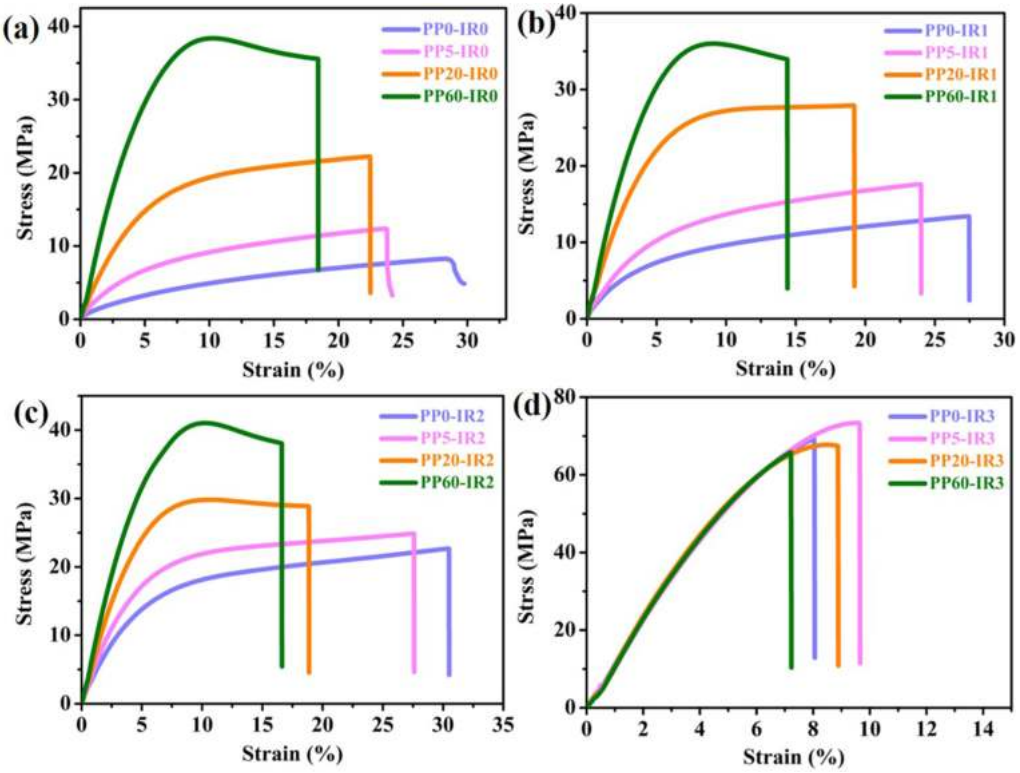

Fig. 6. Stress–strain curves of the post-cured and irradiated specimens. (For interpretation of the references to colour in this figure legend, the reader is referred to the web version of this article.)

3.3. The bond change of the specimens after γ-ray radiation

Infrared spectroscopies of PP60-IRy (y = 0, 1, 2, 3) are shown in Fig. 7, and three peaks with significant changes are magnified. A broad infrared absorption band in the range 3100–3700 cm^{-1} in FTIR spectra is responsible for the O-H and N-H stretching vibrations, and the peaks at 2800–3000 cm^{-1} are ascribed to the stretching vibrations of C-H [34]. Two peaks at 1244 cm^{-1} and 916 cm^{-1} are attributed to epoxy groups [35,36], whose intensity reduce after 1000 KGy γ-ray radiation. The change demonstrates that the γ-rays induce the crosslinking of epoxy. The peaks at 1181 cm^{-1} and 985 cm^{-1} are attributed to ether groups, and that at 1724 cm^{-1} and 1297 cm^{-1} are ester groups [34,37,38]. The two peaks (at 1297 cm^{-1} and 985 cm^{-1}) disappeared after 1000 KGy γ-ray radiation because the γ-rays destroy them. The peaks of CH = CH stretching mode at 1635 cm^{-1} and twisting mode at 810 cm^{-1} are also observed [39,40], whose constant intensity means no free radical polymerization. The position of some peaks changed after 1000 KGy γ-ray radiation. The peaks move towards a lower wavenumber (redshift). The shift is caused by the combined action of the induction effect and conjugation effect. There is no highly electronegative atom or group in the material, the induction effect is weak. Therefore, the redshift is mainly caused by the conjugation effect.

3.4. The surface and cross-section morphologies of the specimens

The effect of γ-rays on morphologies of the samples was demonstrated by the backscattered electron (BSE) mode of scanning electron microscopy. BSE images of surface morphologies and cross-section morphologies of PP60-IR0 and PP60-IR3 are shown in Fig. 8. Some pits on the sample surface are caused by the ink tank of the DLP printer. Beyond that, there is no other difference before and after irradiation. The white arrows in the figures indicate the thickness of the samples, which is about 1 mm. The tensile fracture surfaces of PP60-IR0 and PP60-IR3 are similar in appearance, and both have linear and fish-scale patterns. γ-ray radiation has no obvious effects on the morphologies.

The short GFs are added to improve the mechanical properties of the resin, which has good light transmittance and has little effect on DLP printing and UV light post-curing of the resin. An optical microscope was used to observe the CFs morphology and estimate the fiber length, and the GFs length distribution is shown in Fig. 9(a-b). The average length of the GFs is about 63.2 μm. The cross-section morphology of short GFs reinforced PP60-IR2 is shown in Fig. 9(c). The crack in the section is radioactive, and the crack source is in the middle of the section, which means a mixture of brittle fracture and ductile fracture. Select three positions marked with blue boxes in the section for magnification observation. Both fibers and pores can be observed in the cross-section. The holes are caused by fibers fracture and extraction [41,42]. The fibers are marked with solid circles and the holes with dashed circles as shown in Fig. 9(d-f). The fiber divides the crack into two cracks as it expands, demonstrating that the fibers inhibit crack growth, resulting in the improvement of tensile properties. In addition, interfaces between the printing layers and visible defects are not observed in the cross-section, indicating high interfacial strength and tensile properties [43,44].

Different amounts (0.2 wt%, 0.5 wt%, and 1.0 wt%) of GFs were used to reinforce the PP60-IR2 resin to obtain composites, named PP60-IR2-0.2GF, PP60-IR2-0.5GF, and PP60-IR2-1.0GF. Tan δ and storage modulus curves, stress–strain curves, and thermogravimetric curves of PP60-IR2-0.2GF, PP60-IR2-0.5GF, and PP60-IR2-1.0GF specimens are shown in Figure S4. T_g decreased from 67.0 °C to 64.2 °C, because GFs hindered the formation of the cross-linking networks. The strain at break decreased from 18.4 % to 11.1 %, and the stress increased from 35.6 MPa to 42.7 MPa and increased by 20.0 % with the increasing GFs content. The thermal stability of GFs reinforced composites was also improved. $T_{5\%}$ was increased from 317 °C to 350.5 °C and the carbon yield rate rose from 6.6 % to 10.8 %, which exhibited a significant improvement in thermodynamic properties.

The printed flowers and canister in short GFs doped composite ink are in Figure S5. Different colors of temperature-sensitive powders are

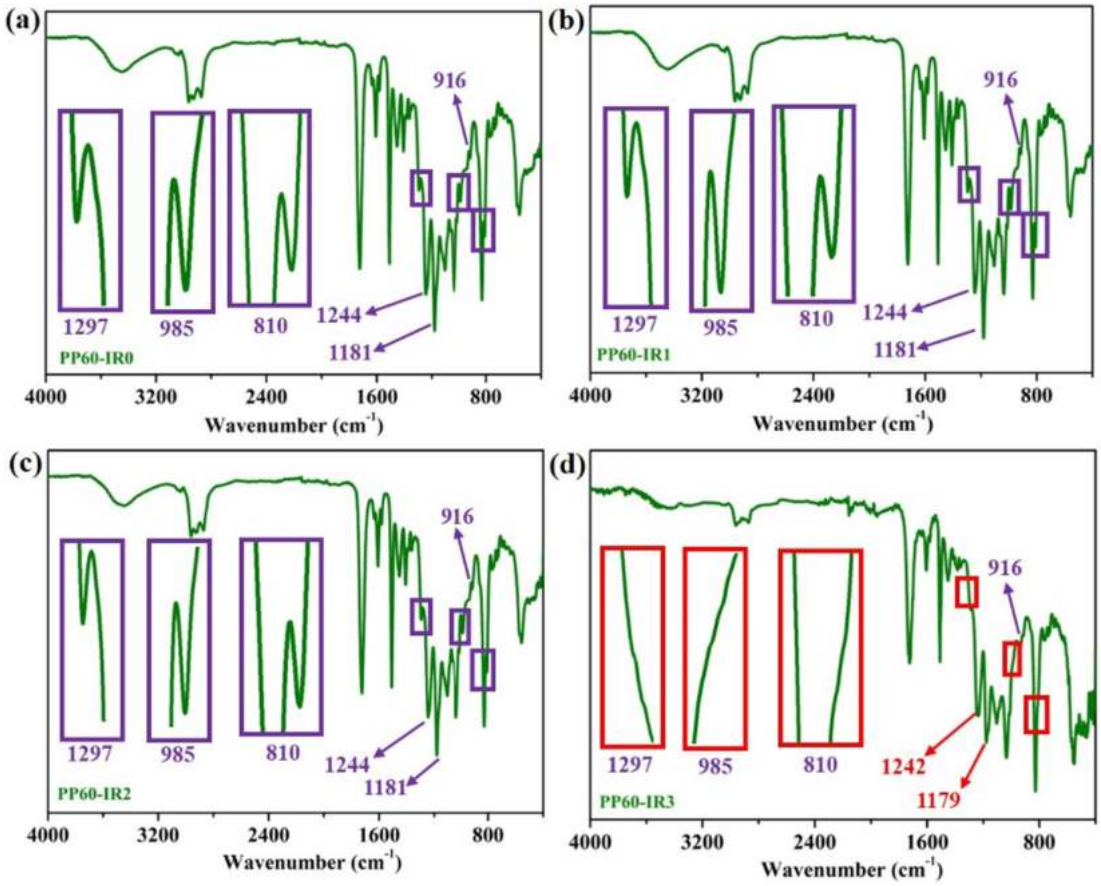

Fig. 7. IR curves of the post-cured and irradiated specimens. (For interpretation of the references to colour in this figure legend, the reader is referred to the web version of this article.)

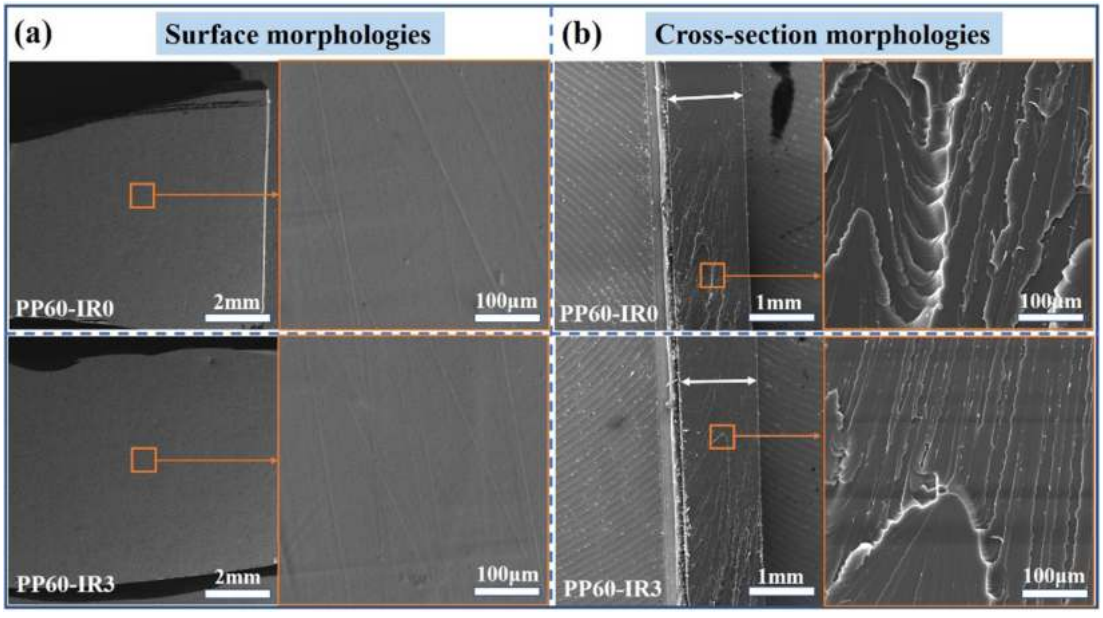

Fig. 8. BSE images: (a) surface morphologies and (b) cross-section morphologies of PP60-IR0 and PP60-IR3. (For interpretation of the references to colour in this figure legend, the reader is referred to the web version of this article.)

added to the composite ink to make the printed specimens beautiful and temperature-sensitive. Surface morphologies of the printed chrysanthemum and canister are shown in Figure S6. The printing layers and short GFs on the surface can be seen in the BSE images of the printed canister.

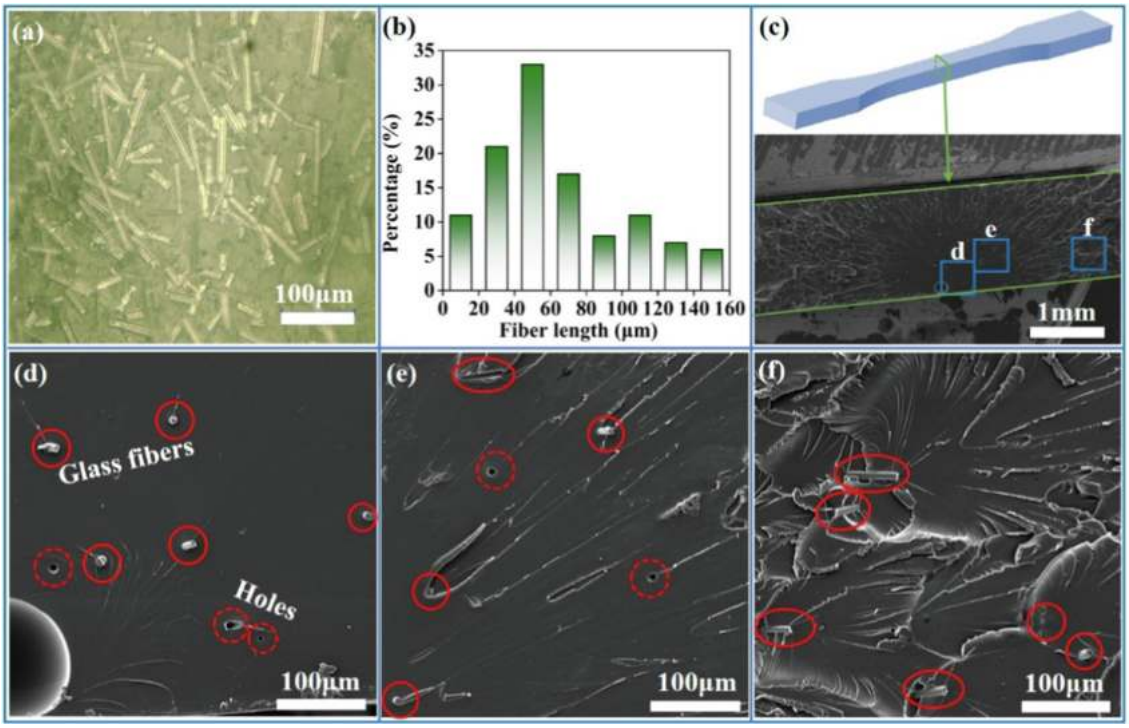

Fig. 9. (a) Fiber morphology observed using an optical microscope; (b) GFs length distribution; (c-f) The cross-section morphology of short GFs reinforced PP60-IR2. (For interpretation of the references to colour in this figure legend, the reader is referred to the web version of this article.)

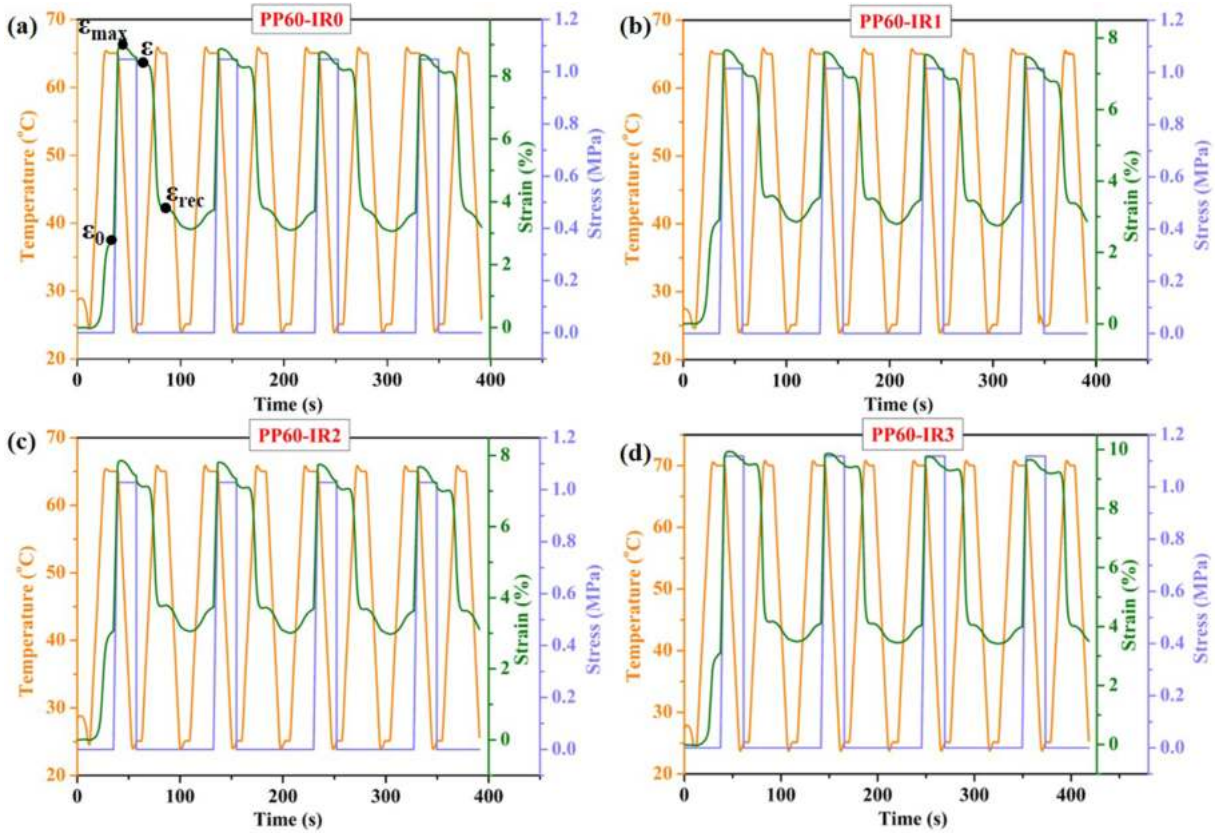

Fig. 10. Shape memory cycles of PP60-IRy (y = 0, 1, 2, 3). (For interpretation of the references to colour in this figure legend, the reader is referred to the web version of this article.)

3.5. Shape memory properties of the specimens after γ-ray radiation

R_f and R_r are two critical indicators to evaluate the shape memory behaviors of the resins, which can be obtained by the shape memory cycle test. Four cycles are tested for each specimen and the results are shown in Fig. 10. The stress is zero and the strain increases during the heating stage of the first cycle, which is caused by the thermal expansion properties of the resin. The strain caused by thermal expansion is labeled the initial strain (ε_0). The highest test temperature is 65 °C for PP60-IR0, PP60-IR1, and PP60-IR2, which is 70 °C for PP60-IR3. The T_g of the specimens determines the highest test temperatures. The strain reaches its maximum under stress and the maximum strain is marked as ε_{max}. When the sample is cooled to 25 °C, the strain reduces slightly after the stress is removed, which was labeled as ε. When the temperature rises to the highest temperature again, the strain decreases to the lowest value labeling ε_{rec}. The Eqs. (2) and (3) are used to calculate R_f and R_r. The data are listed in Table S6. The average R_f of PP60-IR0 is 91.8 % and reduces with increasing γ-ray dose, which is caused by the breaking chain segment between the crosslinking points. The average R_r of PP60-IR0 increased after γ-ray radiation illustrating the increase of shape recovery force, which is attributed to the increase of crosslinking points.

The thermal conductivity of specimens is an essential factor in determining the shape recovery time. Flower fading experiments were carried out in hot water at about 80 °C and schematic diagrams of the flowers are inserted in the upper right side of the pictures as shown in Figure S7. The thickness of chrysanthemum petals is about 0.5 mm and the thickness of the receptacle is about 2 mm. The petals fade in 2 s, the receptacle in 6 s. The 4D printed lotus has thicker petals and receptacles and takes 100 s to fade. The results demonstrate that thin slices are more prone to rapid reshaping and recovery.

A saffron chrysanthemum is selected to demonstrate the shape recovery process. Soak the blooming chrysanthemum in hot water (80 °C) for 10 s, pull the petals together, and cool the flower to room temperature. The gathered flower is cooled to room temperature to complete the formation of the flower from blooming to gathering as shown in Fig. 11. The 4D printed cubic undergoes a deformation from closing to opening, and the canister (in Figure S8) reshapes from standing to twisting. It takes about 20 s for the gathered chrysanthemum to bloom fully and the cubic to close. The shape recovery process of the twisting canister takes only 5 s, much shorter than that of the flower and cubic because of the little distortion of the canister.

4. Conclusion

The UV light-induced network is formed after UV light post-curing of 60 min and the ray-induced network is formed by the crosslinking of epoxy irradiated by 100 KGy γ-rays. The printed IPN resins have the characteristics of low T_g (57.3–82.6 °C) high storage modulus (1.02–4.89 GPa), and high toughness (14.4–30.4 %). The yellowing and thermodynamic degradation of the samples are caused by 1000 KGy γ-ray radiation, which is due to over-curing and destruction of the network structure. The short GFs reinforced composites possess stable R_f and R_r in shape memory cycle testing and the chrysanthemum and canister show rapid shape recovery behaviors. The high-performance IPN composites have a desirable future in manufacturing smart deployable structures, medical devices, automobiles, etc.

CRediT authorship contribution statement

Linlin Wang: Investigation, Data curation, Formal analysis, Writing - original draft. **Fenghua Zhang:** Methodology, Formal analysis, Project administration, Writing - review & editing. **Shanyi Du:** Funding acquisition, Supervision, Writing - review & editing. **Jinsong Leng:** Resources, Project administration, Supervision.

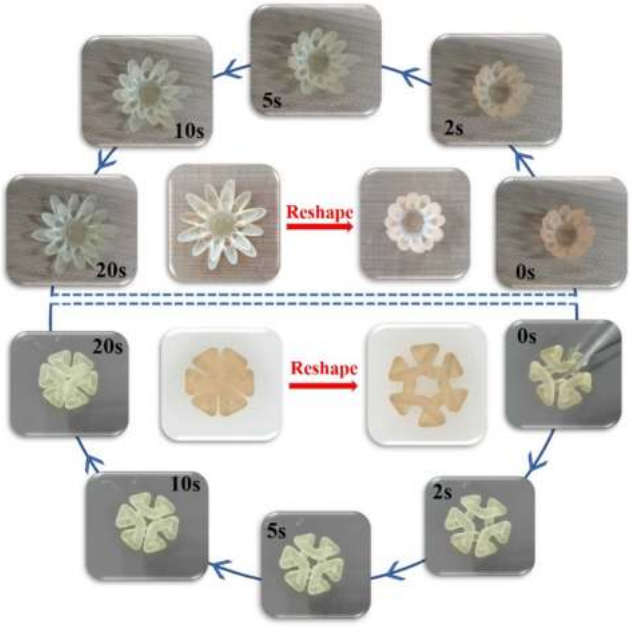

Fig. 11. Shape recovery behaviors of the gathered flower and the opened cubic. (For interpretation of the references to colour in this figure legend, the reader is referred to the web version of this article.)

Declaration of Competing Interest

The authors declare that they have no known competing financial interests or personal relationships that could have appeared to influence the work reported in this paper.

Acknowledgments

This work is supported by the National Natural Science Foundation of China (Grant No. 11632005) and the Heilongjiang Touyan Innovation Team Program.

Appendix A. Supplementary material

Supplementary data to this article can be found online at https://doi.org/10.1016/j.compositesa.2022.107146.

References

[1] Wu XL, Kang SF, Xu XJ, Xiao F, Ge XL. Effect of the crosslinking density and programming temperature on the shape fixity and shape recovery in epoxy-anhydride shape-memory polymers: Article. J Appl Polym Sci 2014;131(15):40559.
[2] Xu W, Pan Yi, Yin Lv, Zheng Z, Deng J, Ding X. Reprocessable shape memory epoxy resin based on substituent biphenyl structure. Macromol Chem Phys 2021;222(10):2000401.
[3] Santiago D, Fabregat-Sanjuan A, Ferrando F, De la Flor S. Recovery stress and work output in hyperbranched poly(ethyleneimine)-modified shape-memory epoxy polymers. J Polym Sci Pol Phys 2016;54(10):1002–13.
[4] Que X, Yan Y, Qiu Z, Wang Y. Synthesis and characterization of trifluoromethyl-containing polyimide-modified epoxy resins. J Mater Sci 2016;51(24):10833–48.
[5] Shiravand F, Ascione L, Persico P, Carfagna C, Brocks T, Cioffi MOH, et al. A novel hybrid linear–hyperbranched poly(butylene adipate) copolymer as an epoxy resin modifier with toughening effect. PolymInt 2016;65(3):308–19.
[6] Xu SA, Song XX, Cai YB. Mechanical Properties and Morphologies of Carboxyl-Terminated Butadiene Acrylonitrile Liquid Rubber/Epoxy Blends Compatibilized by Pre-Crosslinking. Materials 2016;9:640.
[7] Farooq U, Teuwen J, Dransfeld C. Toughening of Epoxy Systems with Interpenetrating Polymer Network (IPN). Polymers 2020;12:1908. https://doi.org/10.3390/polym12091908.
[8] Zhang LX, Jiao HQ, Jiu HF, Chang JX, Zhang SM, Zhao YN. Thermal, mechanical and electrical properties of polyurethane/(3-aminopropyl) triethoxysilane functionalized graphene/epoxy resin interpenetrating shape memory polymer composites. Compos Part A 2016;90:286–95.

[9] Takado K, Ube T, Ikeda T. Photomobile polymer materials with double network structures: crosslinked azobenzene liquid-crystalline polymer/methacrylate composites. Mol Cryst Liq Cryst 2014;601(1):43–8.
[10] Hatta M, Shinya A, Gomi H, Vallittu P, Säilynoja E, Lassila L. Effect of Interpenetrating Polymer Network (IPN) Thermoplastic Resin on Flexural Strength of Fibre-Reinforced Composite and the Penetration of Bonding Resin into Semi-IPN FRC Post. Polymers 2021;13:3200.
[11] Wu CM, Yi R, Liu YJ, He Y, Wang C. Delta DLP 3D Printing with Large Size. In: IEEE/RSJ International Conference on Intelligent Robots and Systems (IROS). Daejeon, October, 2016. p.2155-2160.
[12] Zhu G, Hou Yi, Xu J, Zhao N. Reprintable Polymers for Digital Light Processing 3D Printing. Adv Funct Mater 2021;31(9):2007173.
[13] Zhao Z, Tian X, Song X. Engineering materials with light: recent progress in digital light processing based 3D printing. J Mater Chem C 2020;8(40):13896–917.
[14] Zhu GD, Hou Y, Xu J, Zhao N. Digital Light Processing 3D Printing of Enhanced Polymers via Interlayer Welding. Macromol Rapid Commun 2022;43:2200053. https://doi.org/10.1002/marc.202200053.
[15] Kim SG, Song JE, Kim HR. Development of fabrics by digital light processing three-dimensional printing technology and using a polyurethane acrylate photopolymer. Text Res J 2020;90(7-8):847–56.
[16] Liu Sa, Mo L, Bi G, Chen S, Yan D, Yang J, et al. DLP 3D printing porous β-tricalcium phosphate scaffold by the use of acrylate/ceramic composite slurry. Ceram Int 2021;47(15):21108–16.
[17] Zhang Q, Weng S, Hamel CM, Montgomery SM, Wu J, Kuang X, et al. Design for the reduction of volume shrinkage-induced distortion in digital light processing 3D printing. Extre Mech Lett 2021;48:101403.
[18] Wu D, Zhao Z, Zhang Q, Qi HJ, Fang D. Mechanics of shape distortion of DLP 3D printed structures during UV post-curing. Soft Matter 2019;15(30):6151–9.
[19] Moon W, Kim S, Lim BS, Park YS, Kim JYR, Chung HS. Dimensional accuracy evaluation of temporary dental restorations with different 3D printing systems. Materials 2021;14:1487.
[20] Zhu G, Hou Yi, Xiang J, Xu J, Zhao N. Digital light processing 3D printing of healable and recyclable polymers with tailorable mechanical properties. ACS Appl Mater Inter 2021;13(29):34954–61.
[21] Hanafy TA. Drastic effects of fast neutrons and c-irradiation on the DC conductivity of Co-, Ni-, Mn- and Ag-gelatin doped films. Curr Appl Phys 2008;8:527–34.
[22] Bhat NV, Nate MM, Kurup MB, Bambole VA, Sabharwal S. Effect of c-radiation on the structure and morphology of polyvinyl alcohol films. Nucl Instrum Meth B 2005;237:585–92.
[23] Wang L, Zhang F, Liu Y, Du S, Leng J. photosensitive composite inks for digital light processing four-dimensional printing of shape memory capture devices. ACS Appl Mater Inter 2021;13(15):18110–9.
[24] Marin E, Boschetto F, Zanocco M, Doan HN, Sunthar TPM, Kinashi K, et al. UV-curing and thermal ageing of methacrylated stereo-lithographic resin. Polym Degrad Stabil 2021;185:109503.
[25] Murray MP, Bruckman LS, French RH. Photodegradation in a stress and response framework: poly(methyl methacrylate) for solar mirrors and lens. J Photon Energy 2012;2(1):022004.
[26] Zhang W, Zhang X, Qin Z, Zhang W, Yang R. Mechanical and flame retardant performance of fiberglass-reinforced polysilsesquioxane interpenetrated with poly (ethylene glycol)-urethane. Compos Part A 2021;149:106490.
[27] Dragan ES, Humelnicu D, Ignat M, Varganici CD. Superadsorbents for Strontium and Cesium Removal Enriched in Amidoxime by a Homo-IPN Strategy Connected with Porous Silica Texture. ACS Appl Mater Inter 2020;12(40):44622–38.
[28] Jayaramudu T, Ko H-U, Kim HC, Kim JW, Li Y, Kim J. Transparent and semi-interpenetrating network P(vinyl alcohol)- P(Acrylic acid) hydrogels: pH responsive and electroactive application. Int J Smart Nano Mater 2017;8(2-3):80–94.
[29] Bell LN, Touma DE. Glass Transition Temperatures Determined using a Temperature-Cycling Differential Scanning Calorimeter. J Food Sci 1996;61(4):807–10.
[30] Jana PP, Das J. Precise estimation of glass transition and crystallization temperatures of $Zr_{55}Cu_{30}Ni_5Al_{10}$ metallic glass using step-scan modulated temperature differential scanning calorimeter. Thermochim Acta 2018;660:18–22.
[31] Jana PP, Das J. Accurate measurement of glass transition temperature of Cu47.5Zr47.5Al5 and Zr41.2Ti13.8Cu12.5Ni10Be22.5 using step-scan modulated differential scanning calorimeter. J Alloy Compd 2019;800:314–9.
[32] Park JS, Gwon SJ, Lim YM, Nho YC. Effects of a Radiation Crosslinking on a Drawn Microporous HDPE Film with a Nucleating Agent. Macromol Res 2009;17(8):580–4.
[33] Lim Y-M, Gwon H-J, Park J-S, Nho Y-C, Shim J-W, Kwon IK, et al. Synthesis and Properties of Hyaluronic Acid Containing Copolymers Crosslinked by γ-Ray Irradiation. Macromol Res 2011;19(5):436–41.
[34] Arokiaraj RG, Raju R, Ravikumar S, Sivakumar K, Bhanuprakash P, Pandiyan V. Excess thermodynamic properties and FTIR studies of binary mixtures of aniline with esters at different temperatures. Chem Data Collect 2022;37:100807.
[35] Sawicz-Kryniger K, Niezgoda P, Stalmach P, Starzak K, Wysocka A, Świergosz T, et al. Performance of FPT, FTIR and DSC methods in cure monitoring of epoxy resins. Eur Polym J 2022;162:110933.
[36] Zhang W, Yin L, Zhao M, Tan Z, Li G. Rapid and non-destructive quality verification of epoxy resin product using ATR-FTIR spectroscopy coupled with chemometric methods. Microchem J 2021;168:106397.
[37] Marta W, Enelio TG. The effect of the grafting percentage of starch-g-poly(phenyl acrylate) copolymers on their pyrolysis and kinetics studied by the TG/DSC/FTIR/QMS-coupled method. Polym Degrad Stabil 2017;139:67–75.
[38] Goh KM, Maulidiani M, Rudiyanto R, Abas F, Lai OM, Nyam KL, et al. The detection of glycidyl ester in edible palm-based cooking oil using FTIR-chemometrics and 1 H NMR analysis. Food Control 2021;125:108018.
[39] Oh SJ, Lee SC, Park SY. Photopolymerization and photobleaching of n-butyl acrylate/fumed silica composites monitored by real time FTIR-ATR spectroscopy. Vib Spectrosc 2006;42(2):273–7.
[40] Scherzer T. Depth profiling of the conversion during the photopolymerization of acrylates using real-time FTIR-ATR spectroscopy. Vib Spectrosc 2002;29(1-2):139–45.
[41] Wang P, Zou B, Ding S, Huang C, Shi Z, Ma Y, et al. Preparation of short CF/GF reinforced PEEK composite filaments and their comprehensive properties evaluation for FDM-3D printing. Compos Part B 2020;198:108175.
[42] Peng Y, Yiyun Wu, Wang K, Gao G, Ahzi S. Synergistic reinforcement of polyamide-based composites by combination of short and continuous carbon fibers via fused filament fabrication. Compos Struct 2019;207:232–9.
[43] Li JH, Durandet Y, Huang XD, Sun GY, Ruan D. Additively manufacture d fiber-reinforced composites: A review of mechanical behavior and opportunities. J Mater Sci Technol 2022;119:219–44.
[44] Invernizzi M, Natale G, Levi M, Turri S, Griffini G. UV-Assisted 3D Printing of Glass and Carbon Fiber-Reinforced Dual-Cure Polymer Composites. Materials 2016;9:583.